changed from Mn^{2+} to Mg (as given in Table 1). Image (*b*) in Fig. 5 was then calculated with the beam slightly mistilted according to the diffraction pattern in Fig. 4. The image obtained has a lower symmetry and closely resembles the experimental one. The tail of the dark zig-zag band of octahedra corresponding to positions 11 and 12 is not so dark in this case, but it is impossible to judge from the image which occupancy is the best for octahedron 11. It was possible to match the experimental image of a thicker part of the crystal with an image calculated with an underfocus of −1250 Å and a crystal thickness of 150 Å as can be seen in Fig. 6. Thus it can be concluded that the structural model given in Table 1 is essentially correct, even if some doubt may remain about the cation ordering at certain positions.

Conclusions

This work shows that it is possible to test models of an unknown and complex structure by comparing experimentally obtained electron micrographs with calculated ones. It is of course first necessary to find intuitively a plausible model but this model can be changed by trial and error to give at least an approximate structure which can be very useful as a starting model for a classical X-ray structure determination. It should be of especially good help for compounds like takéuchiite with two long and one short axes.

This work has been supported by grants from the Swedish Natural Science Research Council and National Science Foundation (DMR 78-09197 and DMR 76-06108).

References

ANDERSSON, S. & HYDE, B. (1974). *J. Solid State Chem.* **9**, 92–101.
BOVIN, J.-O. & O'KEEFFE, M. (1980). *Am. Mineral.* In the press.
BOVIN, J.-O. & O'KEEFFE, M. (1981). *Acta Cryst.* A**37**, 35–42.
BOVIN, J.-O., O'KEEFFE, M. & O'KEEFE, M. A. (1981). *Acta Cryst.* A**37**, 28–35.
COWLEY, J. M. & MOODIE, A. F. (1957). *Acta Cryst.* **10**, 609–619.
FEJES, P. L. (1973). Thesis, Arizona State Univ.
GOODMAN, P. & MOODIE, A. F. (1974). *Acta Cryst.* A**30**, 280–290.
KONNERT, J. A., APPLEMEN, D. E., CLARK, J. R., FINGER, L. W., KATO, T. & MIURA, Y. (1976). *Am. Mineral.* **61**, 116–122.
MOORE, P. B. & ARAKI, T. (1974). *Am. Mineral.* **59**, 985–1004.
O'KEEFE, M. A. (1975). Thesis, Univ. of Melbourne.
SKARNULUS, A. D. (1976). Thesis, Arizona State Univ.
TAKÉUCHI, Y. (1956). *Mineral. J.* **2**, No. 1, 19–26.
TAKÉUCHI, Y. (1978). *Recent Prog. Nat. Sci. Jpn*, **3**, 153–181.
TAKÉUCHI, Y., KAGA, N., KATO, T. & MIURA, Y. (1978). *Can. Mineral.* **16**, 475–485.
TAKÉUCHI, Y., WATANABÉ, T. & ITO, T. (1950). *Acta Cryst.* **3**, 98–107.
YAMNOVA, N. Y., SIMONOV, M. A. & BELOV, N. V. (1975). *Sov. Phys. Crystallogr.* **20**, 156–159.

Acta Cryst. (1981). A**37**, 46–51

Self-Crystallizing Molecular Models. VI. Geometrical Supplement

BY TARO KIHARA

University of Electro-Communications, Chofu-shi, Tokyo 182, *Japan*

(*Received* 16 *May* 1980; *accepted* 23 *June* 1980)

Abstract

Magnetic molecular models for simulation of crystal structures are supplemented by calculations based on geometrical idealization of the molecules. An answer is given to the question why solid nitrogen and acetylene present polymorphism whereas carbon dioxide does not. The different crystal structures of SiF_4, CF_4 and SiI_4 and those of UF_6, UCl_6 and WCl_6 are discussed.

0567-7394/81/010046-06$01.00

Introduction

The molecular models with magnetic multipoles reported in this series of papers (Kihara, 1963, 1966, 1970, 1975; Kihara & Sakai, 1978) were invented for the purpose of explaining the crystal structures of non-polar molecules.

If the molecules do not possess any appreciable electric multipoles, the crystal structures are governed

by the condition of closest packing of the molecules. If, on the other hand, the molecules have sufficiently strong electric multipoles, the electrostatic interaction often governs the crystal structure.

The electrostatic multipolar interaction between molecules can be replaced by magnetic interaction between molecular models. The models are made of barium ferrite magnets and plastic pieces. A structure into which these models are assembled will simulate the actual crystal structure.

The model shown in Fig. 1 applies to N_2. The structure into which the models are assembled (Fig. 2) is cubic *Pa*3 simulating the structure of solid nitrogen at low temperatures, the α phase.

Solid nitrogen and solid acetylene present polymorphism. In these and similar cases, our simulation is restricted to structures with lowest electrostatic energies.

The purpose of this paper is to supplement the magnetic molecular models with calculations based on 'geometrical molecular models'.

Nitrogen and acetylene

Under normal pressures, the structure of the α phase of solid nitrogen, which is stable below 35 K, belongs to cubic *Pa*3, the β phase stable at higher temperatures being hexagonal. Under high pressures at low temperatures, the γ phase appears (Swenson, 1955), the structure of which is tetragonal $P4_2/mnm$ (Fig. 3).

The crystal structure of acetylene above 133 K is also cubic *Pa*3. The low-temperature modification has been established by Koski & Sándor (1975) to be

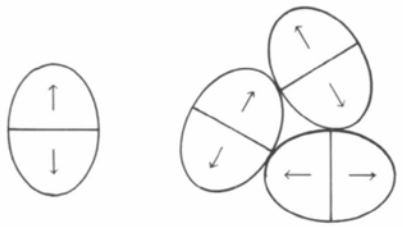

Fig. 1. The magnetic molecular model for N_2.

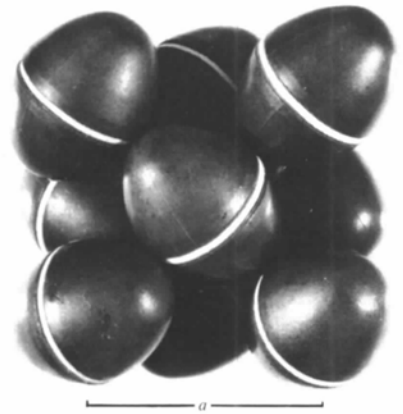

Fig. 2. Cubic *Pa*3 structure simulating the α phase of solid nitrogen.

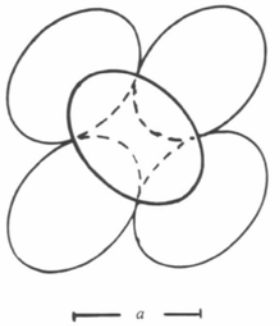

Fig. 3. Tetragonal $P4_2/mnm$ structure of the γ phase of solid nitrogen.

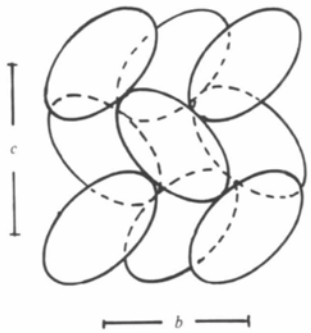

Fig. 4. Orthorhombic *Cmca* structure of the low-temperature phase of solid acetylene.

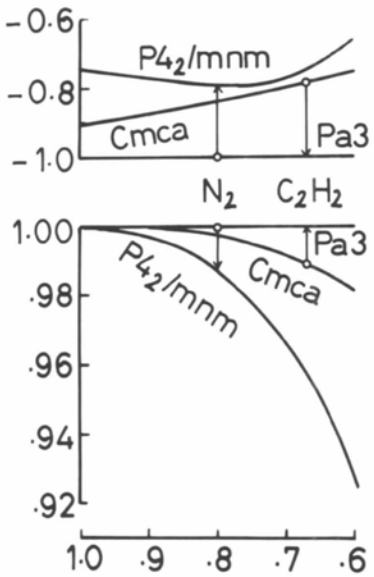

Fig. 5. Relative electrostatic energies (upper half) and molar volumes (lower half) of three solid phases for 'spheroidal molecules' as a function of the axis ratio of the spheroid.

orthorhombic *Cmca*, as shown in Fig. 4, by a neutron powder diffraction study of C_2D_2.

In order to understand such polymorphism, we proceed as follows.

The molecular shape of N_2 or C_2H_2 can be represented by a spheroid. Let the ratio of the minor to the major axis be B; then $B = 0{\cdot}80$ for N_2, and $B = 0{\cdot}67$ for C_2H_2. The electric quadrupole is replaced by a sequence of charges -1, $+2$, -1 (or $+1$, -2, $+1$ for C_2H_2) symmetrically located on the molecular axis. For the end-to-end distance, we choose $1 - B/2$ times the length of the major axis.

Having fixed our 'geometrical molecular model', we calculate the electrostatic energies and molar volumes for the above-mentioned structures, cubic *Pa*3, tetragonal $P4_2/mnm$ and orthorhombic *Cmca*. Fig. 5 shows the results as functions of the axis ratio of the spheroid, the values for *Pa*3 being taken as unity.

In order to draw the electrostatic energies in Fig. 5, it is necessary, and also sufficient, to consider the interaction of a molecule with its twelve nearest and six second neighbors for the cubic structure, and with its corresponding 18 neighbors for the tetragonal and orthorhombic structures.

The electrostatic energy is lowest in the cubic structure, the volume is smallest in the tetragonal structure. This is consistent with the observed α–γ phase transition of solid nitrogen.

In a phase with smaller volume, the energy of the dispersion force will be lower. Hence the three structures are nearly equally favorable in the case of acetylene. This is consistent with the polymorphism presented by solid acetylene.

Carbon dioxide

A spheroid is not appropriate to the molecule of CO_2. This molecule has the shape of a spherocylinder – a parallel body of the line segment defined by the two oxygen atoms. The 'axis ratio' – the ratio of the transverse to the longitudinal diameter – is 0·60 for CO_2. The electric quadrupole is replaced by a symmetric sequence of charges -1, $+2$, -1, the negative charges being at the positions of oxygen atoms.

Performing a similar calculation of electrostatic energies and molar volumes as functions of the axis ratio, we obtain Fig. 6, which is essentially different from Fig. 5. The cubic *Pa*3 structure (*cf.* Fig. 4 of part IV) is most stable both with respect to the electrostatic energy and the volume. This answers the question why solid carbon dioxide does not present polymorphism.

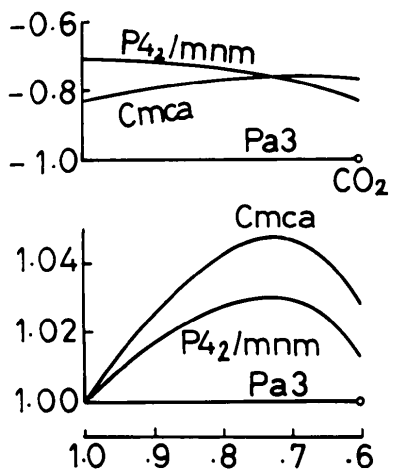

Fig. 6. Curves for 'spherocylindrical molecules' which correspond to Fig. 5.

SiF_4, CF_4, SiI_4, *etc.*

As a geometrical model of the molecules SiF_4, CF_4, SiI_4, *etc.*, we consider a 'regular body of four spheres', a body composed of four spheres in contact in the symmetry of a regular tetrahedron. The electric octopole of the molecule is represented in this model by putting a negative charge -1 at the center of each sphere and a positive charge $+4$ at the center of the body.

The structure with lowest electrostatic energy given by this molecular model is identical to the crystal structure $I\bar{4}3m$ (as shown in Fig. 13 of part III) of SiF_4. This is consistent with the fact that this molecule has an extremely strong electric octopole.

This structure, however, does not assume a closest-packed configuration of the molecular models. The molar volume in this body-centered cubic structure is 32/27 of the molar volume in closest-packing structures.

In closest-packing structures, there are six types of configurations between two neighboring molecules;

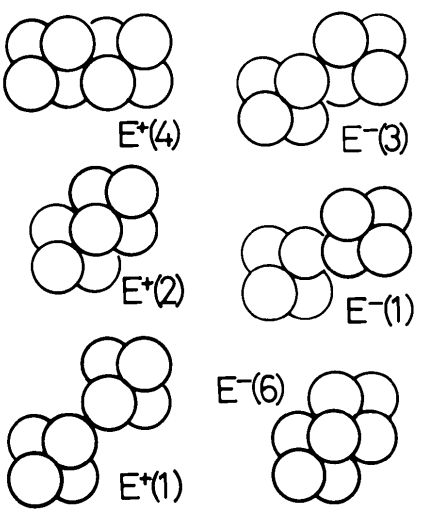

Fig. 7. Six two-body configurations in closest-packing structures of CF_4-type molecules.

these are shown in Fig. 7. The electrostatic energies of each configuration are in the following ratios:

$$E^+(4) = -1{\cdot}00,\ E^-(3) = -0{\cdot}47,\ E^+(2) = -0{\cdot}35,$$

$$E^-(1) = +0{\cdot}08,\ E^+(1) = +0{\cdot}35,\ E^-(6) = +2{\cdot}07.$$

Here $E^+(4)$ denotes that the two molecules in contact at four points can be superposed from one to the other by a parallel translation; and E^- that they can be superposed by a parallel translation after inversion of one of the two.

Relative values of the electrostatic energy per molecule in closest-packing structures are given as follows:

monoclinic $C2/c$:

$$E^+(4) + 3E^-(3) + 2E^+(2) + E^-(1);$$

tetragonal $I\bar{4}2m$:

$$2E^+(4) + 4E^+(2) + 2E^+(1);$$

tetragonal $P4_2/nmc$:

$$E^+(4) + 4E^-(3) + 2E^+(1);$$

orthorhombic $Pban$:

$$2E^+(4) + 2E^-(3) + 2E^-(1) + 2E^+(1);$$

cubic $Pa3$ ($Z = 8$):

$$[6E^-(3) + 6E^+(2) + E^-(6)]/2;$$

cubic $P\bar{4}3m$:

$$3E^+(4) + 6E^+(1).$$

It is to be noted that each sum of the numbers in parentheses is equal to 18, that is $(12 - 3) \times 4/2$.

As compared to the $I\bar{4}3m$ structure of SiF_4, the electrostatic energies are, respectively, 53, 47, 38, 36, 25 and 16%.

The monoclinic $C2/c$, which has the lowest electrostatic energy among closest-packing structures, corresponds to solid carbon tetrafluoride at low temperatures (Bol'shutkin, Gasan, Prokhvatilov & Erenburg, 1972), *cf.* Fig. 12 in part IV.

The cubic $Pa3$ with eight molecules per unit cell corresponds to the crystal structure (Fig. 8) of SiI_4, GeI_4 and SnI_4. The electrostatic octopolar interactions for these molecules seem to play little part.

UF_6, UCl_6 and WCl_6

Our magnetic model of the molecules UF_6, UCl_6 and WCl_6 is shown in Fig. 9; simulations of the crystal structures are given in Figs. 10, 11 and 12.

The shape of these molecules may be idealized by a 'regular body of six spheres', a body composed of six spheres contacting in the symmetry of a regular octahedron. The electric multipole of the molecule is represented in this model by putting a charge -1 at the center of each sphere and a charge $+6$ at the center of the body. The orthorhombic $Pnma$ of UF_6, the trigonal $P\bar{3}m1$ structure of UCl_6 and the trigonal $R\bar{3}$ structure of WCl_6 assume closest-packed configurations of such molecular methods.

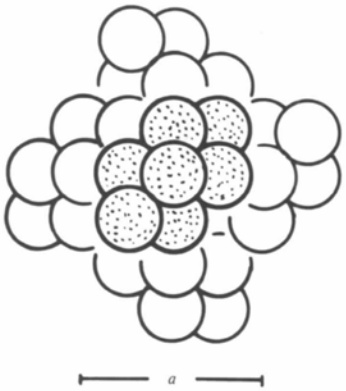

Fig. 8. Cubic crystal structure $Pa3$ ($Z = 8$) of SiI_4-type molecules.

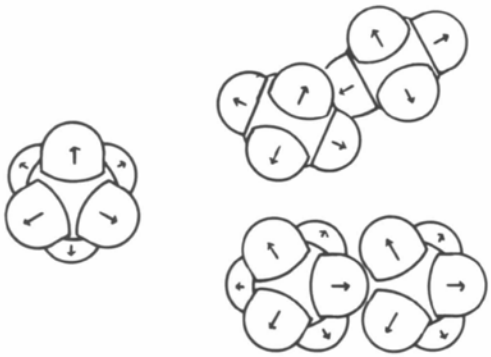

Fig. 9. The molelcular model for UF_6, UCl_6 or WCl_6. The parts with arrows are ferrite magnets; those without arrows are plastic pieces.

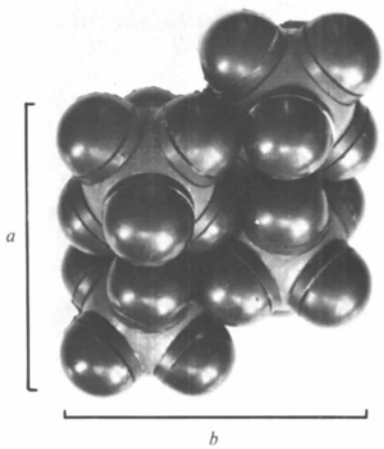

Fig. 10. Orthorhombic $Pnma$ structure simulating the crystal structure of UF_6.

In these closest-packing structures, there are eight types of configurations between two neighboring molecules; these are shown in Fig. 13. The electrostatic energies of each configuration are in the ratios

$$E^-(3) = -1{\cdot}00,\ E^+(5) = -0{\cdot}96,\ E^-(2) = -0{\cdot}43,$$

$$E^+(3) = -0{\cdot}32,\ E^-(5) = -0{\cdot}24,\ E_1^+(1) = -0{\cdot}11,$$

$$E_2^+(1) = +0{\cdot}22,\ E^+(6) = +0{\cdot}54.$$

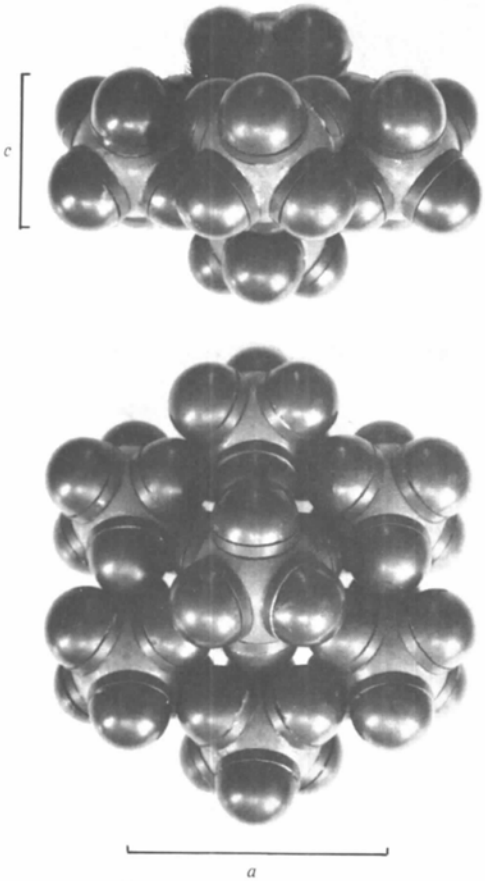

Fig. 11. Trigonal $P\bar{3}m1$ structure simulating the crystal structure of UCl_6.

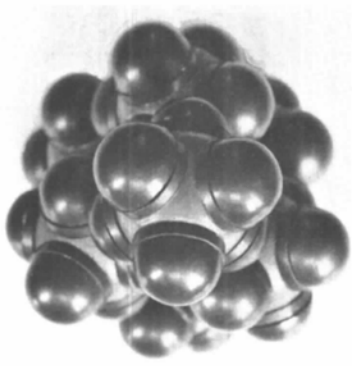

Fig. 12. Trigonal $R\bar{3}$ structure simulating the crystal structure of WCl_6.

Here E^+ denotes that the two molecules can be superposed from one to the other by a parallel translation; E^- that they can be superposed by a parallel translation after reflection of one molecule with respect to a plane perpendicular to the threefold rotary–inversion axis.

Electrostatic energies per molecule are as follows: orthorhombic *Pnma*:

$$2E^-(3) + 2E^+(5) + E^-(2) + E^-(5) + E_1^+(1);$$

trigonal $P\bar{3}m1$:

$$4E^-(3) + E^+(5) + E_2^+(1) + E^+(6);$$

trigonal $R\bar{3}$

$$3E^+(5) + 3E^+(3).$$

Each sum of the numbers in parentheses is equal to 24. In comparison with *Pnma*, the $P\bar{3}m1$ structure is 90% and $R\bar{3}$ is 81%.

The shapes of the molecules of UF_6, UCl_6 and WCl_6 are similar, but the strengths of the electric multipoles are substantially different. Clearly the multipole of the UF_6 is the strongest, which is consistent with the result that its crystal structure has the lowest electrostatic energy.

Since the ionization energies of U and W are 6 and 8 eV, respectively, the multipole of WCl_6 is considered to be weaker than that of UCl_6. In fact, the electrostatic interaction does not seem to play an important role in the crystal of tungsten hexachloride.

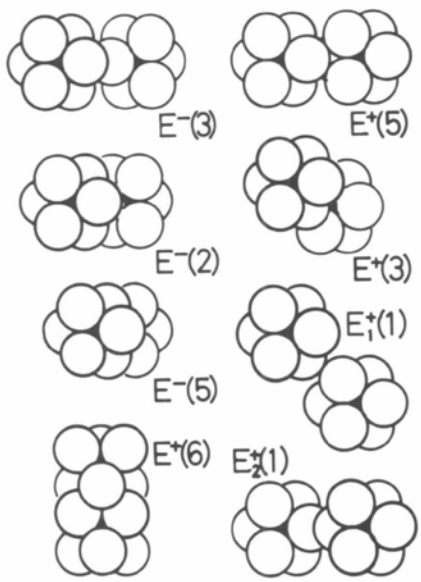

Fig. 13. Eight two-body configurations in closest-packing structures of UF_6-type molecules.

References

BOL'SHUTKIN, N. D., GASAN, V. M., PROKHVALTILOV, A. I. & ERENBURG, A. I. (1972). *Acta Cryst.* B**28**, 3542–3547.
KIHARA, T. (1963). *Acta Cryst.* **16**, 1119–1123.
KIHARA, T. (1966). *Acta Cryst.* **21**, 877–879.
KIHARA, T. (1970). *Acta Cryst.* A**26**, 315–320.
KIHARA, T. (1975). *Acta Cryst.* A**31**, 718–721.
KIHARA, T. & SAKAI, K. (1978). *Acta Cryst.* A**34**, 326–329.
KOSKI, H. K. & SÁNDOR, E. (1975). *Acta Cryst.* B**31**, 350–353.
SWENSON, C. A. (1955). *J. Chem. Phys.* **23**, 1963–1964.

Acta Cryst. (1981). A**37**, 51–61

Irradiation-Induced Defects in β''-Alumina Examined by 1 MV High-Resolution Electron Microscopy

BY YOSHIO MATSUI AND SHIGEO HORIUCHI

National Institute for Researches in Inorganic Materials, Sakura-mura, Niihari-gun, Ibaraki 305, *Japan*

(*Received* 26 *April* 1979; *accepted* 26 *June* 1980)

Abstract

The defect blocks formed in β''-alumina by electron irradiation are examined by 1 MV high-resolution electron microscopy. In order to explain the fact that two distinctly different types of defect images appear even in a single 1 MV micrograph, a new structural model is constructed in place of the two models so far reported. In the model proposed, two spinel-like blocks on either side of the eliminated conduction plane are directly combined by the vectors including x,y components to form cubic close packing of oxygen layers in the resultant defect blocks. The arrangements of cations in the defect block are slightly different from those expected from the spinel structure.

Introduction

The name β''-alumina was first used by Yamaguchi & Suzuki (1968) for the compound $Na_2O.5Al_2O_3$ (or $K_2O.5Al_2O_3$), because the crystal structure was substantially similar to that of β-alumina, $Na_2O.11Al_2O_3$. It was later found that the β''-alumina phase is considerably stabilized by the addition of a small amount of MgO and even single crystals have been prepared (Bettman & Peters, 1969; Kummer, 1972). Such MgO-stabilized β''-alumina, $Na_2O.MgO.5Al_2O_3$, has the idealized crystal structure as shown in Fig. 1(*a*) and (*b*) (Bettman & Peters, 1969). It is constructed by the alternate stacking of the spinel-like blocks and so-called conduction planes which consist of Na_2O. The space group is $R\bar{3}m$ (a = 5·614 and c = 33·85 Å), and the unit cell contains three spinel-like blocks which are mutually related by

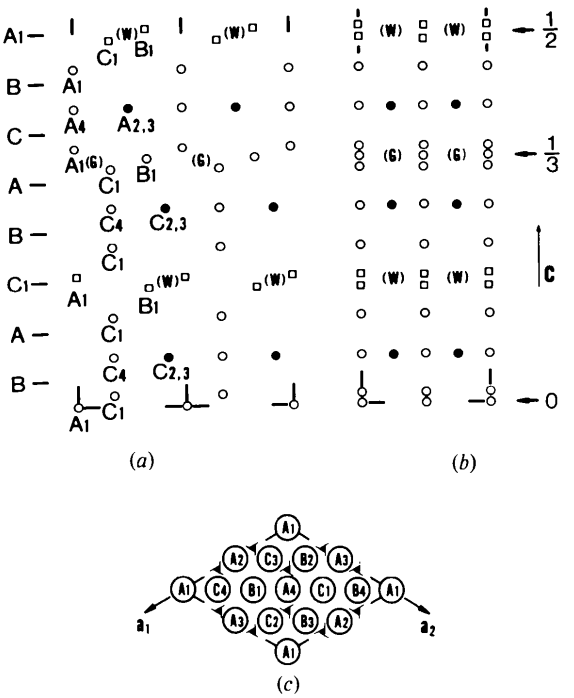

Fig. 1. Schematic representations of the crystal structure of MgO-stabilized β''-alumina, $Na_2O.MgO.5Al_2O_3$. The space group is $R\bar{3}m$ with lattice parameters a = 5·61 and c = 33·9 Å. (*a*) and (*b*) are the projections normal to the (110) and (100) planes, respectively. Half the unit cell is shown in each figure and the remaining half can be derived from the operation of the threefold screw axes shown in (*c*). Squares mean sodium atoms. Empty and filled circles represent Al atoms partly replaced by Mg ones; cations in the full circles are arrayed twice as densely as those in the empty circles along the direction of projection. The oxygen positions are abbreviated but their stacking sequence is indicated at the left-hand side of (*a*). The (x,y) coordinates of each atom can be read out from (*c*).

0567-7394/81/010051-11$01.00